


# Regulation of Microtubule Stability in Pulmonary Microvascular Endothelial Cells in Rats with Severe Acute Pancreatitis: Qingyi Decoction is a Potential CDK5 Inhibitor

Yinan Cao<sup>1-3,\*</sup>, Fan Li<sup>1-3,\*</sup>, Zhenxuan Sun<sup>1-3</sup> , Jin Liu<sup>1-3</sup>, Jie Liu<sup>1-3</sup>, Qi Yang<sup>1-3</sup>, Peng Ge<sup>1-3</sup>, Yalan Luo<sup>1-3</sup> , Hailong Chen<sup>1-3</sup>

<sup>1</sup>Department of General Surgery, The First Affiliated Hospital of Dalian Medical University, Dalian, Liaoning, 116011, People's Republic of China;

<sup>2</sup>Institute (College) of Integrative Medicine, Dalian Medical University, Dalian, Liaoning, 116044, People's Republic of China; <sup>3</sup>Laboratory of Integrative Medicine, The First Affiliated Hospital of Dalian Medical University, Dalian, Liaoning, 116011, People's Republic of China

\*These authors contributed equally to this work

Correspondence: Yalan Luo; Hailong Chen, Department of General Surgery, The First Affiliated Hospital of Dalian Medical University, Zhongshan Road 222, Dalian, 116011, Liaoning, People's Republic of China, Tel +86-411-83635963, Fax +86-411-83622844, Email luoyalanxueshu@163.com; chen hailong@dmu.edu.cn

**Purpose:** Explore the therapeutic effects and regulatory mechanism of Qingyi Decoction (QYD) on severe acute pancreatitis (SAP) associated acute lung injury (ALI).

**Methods:** We identified the constituents absorbed into the blood of QYD based on a network pharmacological strategy. The differentially expressed genes from the GEO database were screened to identify the critical targets of QYD treatment of SAP-ALI. The SAP-ALI rat model was constructed. Some methods were used to evaluate the efficacy and mechanism of QYD in treating SAP-ALI. LPS-stimulated pulmonary microvascular endothelial cell injury simulated the SAP-induced pulmonary endothelial injury model. We further observed the therapeutic effect of QYD and CDK5 plasmid transfection on endothelial cell injury.

**Results:** 18 constituents were absorbed into the blood, and 764 targets were identified from QYD, 25 of which were considered core targets for treating SAP-ALI. CDK5 was identified as the most critical gene. The results of differential expression analysis showed that the mRNA expression level of CDK5 in the blood of SAP patients was significantly up-regulated compared with that of healthy people. Animal experiments have demonstrated that QYD can alleviate pancreatic and lung injury inflammatory response and reduce the upregulation of CDK5 in lung tissue. QYD or CDK5 inhibitors could decrease the expression of NFAT5 and GEF-H1, and increase the expression of ACE-tub in SAP rat lung tissue. Cell experiments proved that QYD could inhibit the expression of TNF- $\alpha$  and IL-6 induced by LPS. Immunofluorescence results suggested that QYD could alleviate the cytoskeleton damage of endothelial cells, and the mechanism might be related to the inhibition of CDK5-mediated activation of NFAT5, GEF-H1, and ACE-tub.

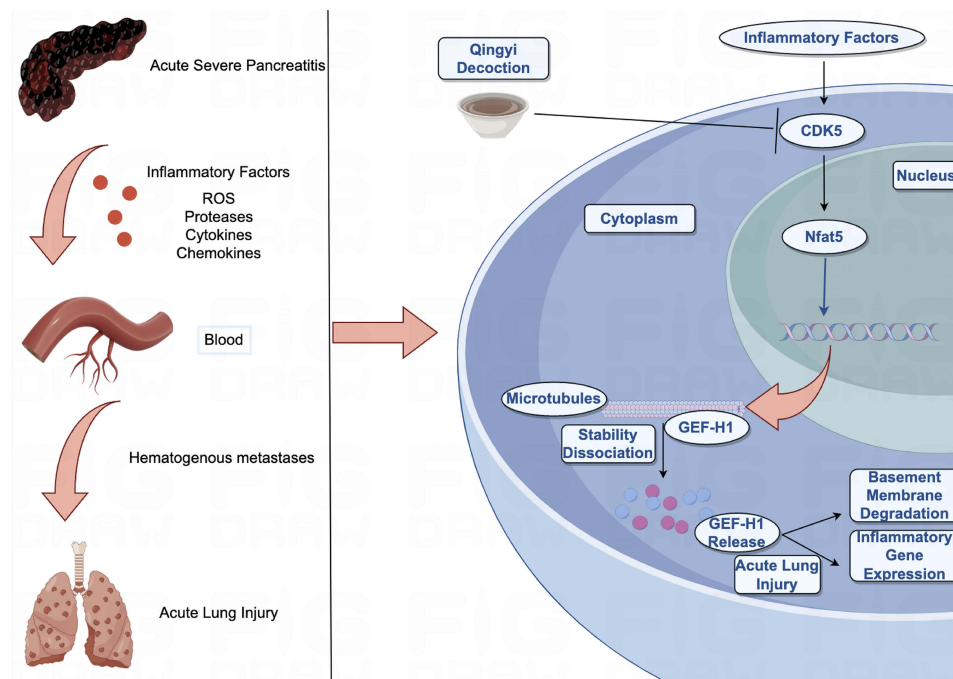
**Conclusion:** CDK5 has been identified as a critical target for pulmonary endothelial injury of SAP-ALI. QYD may partially alleviate microtubule disassembly by targeting the CDK5/NFAT5/GEF-H1 signaling pathway, thus relieving SAP-induced pulmonary microvascular endothelial cell injury.

**Keywords:** Qingyi decoction, severe acute pancreatitis, acute lung injury, CDK5, microtubule

## Introduction

Acute pancreatitis (AP), as one of the most common diseases in general surgery, is an acute inflammatory disease caused by exocrine dysfunction of the pancreas, with the main etiological factors originating from gallstones, heavy alcohol consumption, high triglyceride levels, and immune dysfunction.<sup>1,2</sup> AP is usually classified as mild, moderately severe, and severe acute pancreatitis (SAP), and patients with mild AP have a better prognosis and lower mortality. However,

## Graphical Abstract



approximately 20% of patients develop SAP, which is often associated with more severe systemic inflammatory response syndrome (SIRS) and multiple organ dysfunction syndrome (MODS), with a mortality rate ranging from 15% to 35%.<sup>3,4</sup> Acute Lung Injury (ALI) Acute lung injury (ALI) is the most common and systemic complication of early onset SAP, with a prevalence of 27.7% and a mortality rate of 60%.<sup>5</sup> However, the pathophysiology associated with SAP-ALI has yet to be fully elucidated. Given the high mortality rate of SAP-ALI, it is essential to actively study the molecular mechanisms of disease initiation and progression and provide valuable experience for clinical treatment.<sup>6</sup>

Cell cycle protein-dependent kinase 5 (CDK5) is a proline-directed serine/threonine kinase first described as playing a vital role in the central nervous system.<sup>7</sup> CDK5 is ubiquitously expressed in mammalian tissues and phosphorylates a wide range of proteins, and cellular processes regulated by CDK5 include cytoskeletal dynamics (actin and microtubule dynamics), transcription, apoptosis and senescence.<sup>8,9</sup> The absence of CDK5 in macrophages has been shown to improve the anti-inflammatory response during endotoxemia.<sup>10</sup> The Nuclear factor 5 of activated T cells (NFAT5), also known as tension-responsive enhancer-binding protein (TonEBP), is a member of the Rel family of transcription factors, which includes nuclear factor kappa B (NF- $\kappa$ B) and NFAT1-4, and although NFAT5 was initially identified as a critical component of cellular osmotic homeostasis,<sup>11</sup> it can also be stimulated independently of osmotic pressure by, for example, biomechanical stretching, hypoxemia, inflammatory stimuli, cytokines and reactive oxygen species. Related studies have shown that NFAT5 deficiency attenuates formalin-induced inflammatory pain via the rapamycin-targeting protein (mTOR) signaling pathway.<sup>12</sup> The cytoskeleton (cytoskeleton) is a network of proteins and proteins that form a network of skeletons that act as arteries for intracellular transport of materials and movement of organelles. The main components of the cytoskeleton are microtubules, microfilaments, and intermediate filaments. Relevant studies have demonstrated that Toll-like receptor 2 (TLR2)-specific hemodynamic profiles recruit leukocytes to the choroid plexus in response to inflammation, which then remodels the cytoskeleton of basement membranes and epithelial cells to promote leukocyte migration, opening new avenues for the study of neuroinflammation.<sup>13</sup> Guanine nucleotide exchange factor-H1 (GEF-H1) is a microtubule-associated protein. Coupled with RhoA guanosine triphosphatase GTPase activation via

microtubule dynamics, GEF-H1 activation is implicated in multiple cellular processes such as cell shape, polarisation, differentiation, motility, cell cycle regulation, and epithelial barrier permeability.<sup>14,15</sup>

Qingyi decoction (QYD), a traditional Chinese medicine (TCM) that has been used clinically to treat patients with SAP, consists of eight herbs, including *Bupleurum chinense* DC, *Corydalis yanhusuo*, *Scutellaria baicalensis* Georgi, *Gardenia jasminoides* J. Ellis, *Paeonia lactiflora* Pall., *Rheum officinale* Baill., *Aucklandia costus* Falc., and  $\text{Na}_2\text{SO}_4 \cdot 10 \text{H}_2\text{O}$ .<sup>16</sup> QYD plays a crucial role in anti-inflammatory, antioxidant, and immunomodulation. Current studies have shown that QYD reduces systemic inflammation in SAP by inhibiting the activation of high mobility group box-1 (HMGB1), nucleotide-binding oligomeric domain-like receptor protein-3 (NLRP3), and regulating the expression of secretory phospholipase A2 and G-protein-coupled bile acid receptors.<sup>17–19</sup> However, given the multi-component, multi-target, and multi-pathway action characteristics of QYD, the mechanism of its treatment of SAP-ALI still needs to be further elucidated. Roscovitine is commonly referred to as a “selective inhibitor of cyclin-dependent kinases” and is one of the most favored CDK inhibitors. It substantially inhibits CDC2, CDK2, and CDK5 (with IC<sub>50</sub> values of 0.65, 0.7, and 0.2  $\mu\text{M}$ , respectively). Besides its extensive use in cell cycle and neuronal function experiments, it is also currently being assessed as a potential therapeutic for cancer, viral infections, and inflammatory responses. Therefore, we have chosen Roscovitine as the positive control for the treatment group.

In this study, we identified the constituents absorbed into the blood of QYD and critical targets for treating SAP-ALI based on network pharmacological strategies. By constructing *in vivo* and *in vitro* models, HE staining, immunofluorescence, ELISA, qPCR, and Western Blot methods were used to evaluate the efficacy and mechanism of QYD in treating SAP-ALI.

## Materials and Methods

### Reagents and Antibodies

Antibodies against CDK5 (CAT#A23502), GAPDH Rabbit pAb (CAT#AC001), and Horseradish Peroxidase (HRP)-coupled Anti-Rabbit IgG Antibody (CAT#AS014) were purchased from ABclonal (Wuhan, China). NFAT5 (CAT#ER65748) was purchased from HUABIO (Zhejiang, China). GEF-H1 (CAT#AF4783) and Acetyl-alpha Tubulin (CAT#AF4351) were purchased from Affinity (Liyang, China). Antibodies against immunofluorescence CDK5 (CAT# 14145) and Acetyl-alpha-Tubulin (CAT#35652) were purchased from CST (USA); NFAT5 (CAT# sc-398171) was purchased from Santa Cruz Biotechnology (USA); rhodamine-labeled ghost pen cyclic peptides (TRITC Phalloidin, CAT# BL1189A) was purchased from Biosharp (Hefei, China). Rat tumor necrosis factor- $\alpha$  (TNF- $\alpha$ , Cat#F3768) and interleukin-6 (IL-6, Cat#F15870) were obtained from Xitang Biotechnology (Shanghai, China). The amylase assay kit (CAT#C016-1-1) was obtained from Nanjing Jiancheng Bioengineering Institute (Nanjing, China).

### Preparation of qingyi Decoction and Hydrated Extracts

The raw materials of QYD herbs were provided by the First Affiliated Hospital of Dalian Medical University (Dalian, Liaoning, China), and the main ingredients were *Bupleurum chinense* DC (Chai Hu in Chinese, 15 g), *Corydalis yanhusuo* (Yan Hu Suo in Chinese, 15 g), *Scutellaria baicalensis* Georgi (Huang Qin in Chinese, 12 g), *Gardenia jasminoides* J. Ellis (Zhi Zi in Chinese, 15 g), *Paeonia lactiflora* Pall. (Bai Shao in Chinese, 15 g), *Rheum officinale* Baill. (Da Huang in Chinese, 20 g), *Aucklandia costus* Falc. (Mu Xiang in Chinese, 15 g), and  $\text{Na}_2\text{SO}_4 \cdot 10 \text{H}_2\text{O}$  (Mang Xiao in Chinese, 10 g), soaked with deionized water, weighed 10 times their total weight for 30 min, boiled for 1 h, and filtered. Then, the residual herbs were continued to be decocted with 8 times the total weight of water for 30 min and then filtered, then  $\text{Na}_2\text{SO}_4 \cdot 10 \text{H}_2\text{O}$  was added, and the two times filtrate was mixed and concentrated to 1 g/mL, sterilize, and then bottled and stored in a refrigerator at 4°C. The hydrated extracts were the final concentration of the 2 times filtrate converted into the final concentration of the extracts, and the yield of the extracts was 29.5% and was kept in a desiccator before use. The chemical profiles of QYD mapped using ultra-performance liquid chromatography coupled with quadrupole time-of-flight mass spectrometry are presented in the previous study.<sup>16</sup>

## CDK5 Gene Identification and Exploration

The dataset GSE194331 was downloaded from the GEO public database (<http://www.ncbi.nlm.nih.gov/geo>). DEGs (differentially expressed genes) were identified using the DESeq2 package in R. Genes that met the criteria ( $|\log_2\text{FoldChange}| \geq 1$ ,  $p_{\text{adj}} < 0.05$ ) were defined as DEGs. Transcriptional data was dimensionally reduced and clustered using the UMAP package in R, and data visualization was performed using the ggplot2 package.

## Network Pharmacology Analysis

The constituents absorbed into the blood of QYD were selected via a screening process using TCMSP and earlier mass spectrometry data. The databases used for screening potential targets of prototype components were TCMSP, DrugBank (<https://www.drugbank.com/>), SwissTargetPrediction (<http://www.swisstargetprediction.ch/>), and SuperPred (<https://prediction.charite.de/>). Utilize the UniProt database (<https://www.uniprot.org/>) to standardize gene names. The prototype components and targets of QYD were loaded into the Cytoscape 3.9.1 program in order to construct the “Component-target” network. The DAVID database (<https://david.ncifcrf.gov/>) was used to perform gene ontology (GO) and Kyoto Encyclopedia of Genes and Genomes (KEGG) pathway enrichment analysis.<sup>20</sup> The GeneCards (<https://www.genecards.org/>), Disgenet (<https://www.disgenet.org/>), and TTD database (<http://db.idrblab.net/ttd/>) were used to ascertain genes associated with SAP. Retrieve protein-protein interaction data from the String (<https://cn.string-db.org/>) database.

## Molecular Docking

Previous studies have shown that CDK5 plays a key role in the occurrence and development of AP.<sup>21</sup> We further identified the binding activity of 18 prototype components of Qingyi Decoction with CDK5. The PDB database (<https://www.rcsb.org>) was used to obtain the 3D crystal structures of CDK5. PubChem database (<https://pubchem.ncbi.nlm.nih.gov>) was used to retrieve the three-dimensional structure of 18 compounds. Import the constituents and target into the AutoDock Vina software, then perform dehydration and hydrogenation preprocessing and designate them as the receptor and ligand, respectively.<sup>22</sup> When the binding energy of the ligand-target complex is less than or equal to  $-5$  kJ/mol, it suggests that the interaction between them can occur spontaneously. The 3D conformation of the ligand-receptor was displayed by Pymol software.

## Animal Preparation and Experimental Protocols

All animal experiments were conducted in accordance with the Guidelines for the Care and Use of Laboratory Animals developed by the National Institutes of Health, USA, and were carried out according to the experimental protocols approved by the Research and Animal Ethics Committee of Dalian Medical University (Dalian, China) (approval number: AEE19003). Male Sprague-Dawley rats, 180–220 g, were obtained from Sprague-Dawley (Beijing) Biotechnology Co. They will be acclimatized and fed in a pathogen-free room at a consistent temperature of 20–22°C, with light and dark cycles of 12 h, respectively, and allowed free access to standard rat food and water. The rat model of SAP-ALI was established by acclimatizing and feeding for one week before modeling. Then, 40 rats were randomly divided into four groups: sham-operated group (SO), severe acute pancreatitis model group (SAP), severe acute pancreatitis model + inhibitor group (SAP+Roscovitine), and severe acute pancreatitis model + pancreatic cleansing soup group (SAP+QYD) ( $n = 10$ , in each group). The experimental rats were injected retrogradely with 5.0% sodium taurocholate (STC, 50 mg/kg, 0.1 mL/min) into their biliopancreatic ducts<sup>18</sup> In the SAP+Roscovitine group, intraperitoneal injection of the inhibitor was given after modeling and then the abdomen was closed (16.5 mg/kg). In the SAP+QYD group, 4 hours and 12 hours after retrograde injection into the biliopancreatic duct, the rats were treated with QYD via gavage (10 g/kg, bioavailability: 1 g/mL). All rats were anesthetized with 1% sodium pentobarbital (4 mg / 100 g). They were executed after 24 h. Bronchoalveolar lavage fluid (BALF), blood samples from the abdominal aorta, dissected pancreas, and lung tissues were collected and stored at  $-80^\circ\text{C}$ . The remaining pancreas and lung tissues were embedded in paraffin after fixation in 10% formalin.

## Measurement of Serum Amylase, Interleukin-6, Tumor Necrosis Factor- $\alpha$

We assayed amylase in rat serum by spectrophotometry using commercial kits. Rat serum levels of tumor necrosis factor- $\alpha$  (TNF- $\alpha$ ) and interleukin-6 (IL-6) were assessed using enzyme-linked immunosorbent assay (ELISA) kits according to the manufacturer's instructions.

## Measurement of Pulmonary Vascular Permeability

The trachea and esophagus of the rats were separated by blunt separation, and all wet lung tissue weights were obtained and calculated. Then, the lung tissue was placed in a 60°C drying oven for 48 h to dry the lung water, and its dry weight was measured. Pulmonary vascular permeability was evaluated using the wet/dry weight (W/D) ratio.

Firstly, the rat trachea was completely isolated and dissected out, and then a lavage needle was inserted into the left lung through the main bronchus; the right main bronchus was ligated with a surgical suture, and normal saline was injected, 5mL each time, and the left bronchoalveolar lavage fluid (BALF) was collected about 1 min later. The above steps were repeated three times to obtain the total BALF of the lungs. Finally, BALF was centrifuged (4°C at 3000 rpm for 10 min) to separate the supernatant and stored at -80°C.

In addition, we used the Evans blue dye assay. 2 h before sampling, Evans blue dye (Shanghai McLean Biochemical Technology Co., Ltd.) was injected into rats through the tail vein. After sampling, the tissues were treated with formamide (Shanghai McLean Biochemical Technology Co., Ltd.) in a 37°C water bath for 48 h. Finally, the concentration of Evans blue dye in lung tissues was determined by spectrophotometer at 620 nm.

## Histological Examination

Isolated pancreatic and lung tissues were fixed in 10% paraformaldehyde for 24 h. The tissues were embedded in paraffin and cut into 5  $\mu$ m thick sections. Sections were routinely stained with hematoxylin and eosin (HE). Tissues were scored under a light microscope by a pathologist unaware of the experimental design. The following parameters (alveolar necrosis, inflammation, hemorrhage, and edema) were used to determine the pancreatic histological score (scores from 0 to 4), inflammatory cell infiltration, bleeding, and alveolar septal thickening were used as parameters for scoring the lung tissues (scores from 0 to 3). The total scores of the above parameters were calculated separately, evaluating specimens from a minimum of three rats in each group.<sup>23–25</sup>

## Western Blot Analysis

A protein extraction kit (KeyGen, KGI Biotechnology, Nanjing, China) was used to achieve protein extraction and quantification of rat lung tissue. Protein samples were separated by 8–12% sodium dodecyl sulfate-polyacrylamide gel electrophoresis and electrotransferred onto a 0.22 $\mu$ m polyvinylidene difluoride membrane. The membranes were closed with 5% skimmed milk solution for 2 h at room temperature and then incubated overnight at 4 °C with primary antibodies: CDK5 (1:1000), NFAT5 (1:500), GEF-H1 (1:500), Acetyl- $\alpha$  Tubulin (1:1000), and GAPDH (1:30,000). After washing with TBST solution, the membranes were incubated with HRP-conjugated secondary antibody (1:10,000) for 1 h at room temperature. A chemiluminescence system (Tanon-5200, Shanghai, China) and ImageJ software were used to analyze band intensities normalized to GAPDH statistically.

## Quantitative Real-Time Polymerase Chain Reaction (PCR)

RNA was extracted from rat lung tissues using RNAex Pre-Reagent (AG21102, Accurate Biology, Changsha, China). Single-stranded mRNA obtained was reverse transcribed to cDNA using Evo M-MLV Reverse Transcription Hybrid Kit (AG11728, Accurate Biology). Synthesized cDNA was amplified by SYBR<sup>®</sup> Green Premix Pro Taq HS qPCR kit II (AG11702, Accurate Biology) for amplification.  $2^{-\Delta\Delta C_t}$  This method was used for the statistical analysis of mRNA levels of the housekeeping gene GAPDH. The details of the gene sequence can be seen in [Supplementary File S1](#).

## Cell Culture and Experimental Design

Rat pulmonary microvascular endothelial cells (R-PMVECs, CAT#PC-150r) were purchased from Wuhan Sciencell Biotechnology Co. Ltd (Wuhan, China). Endothelial Cell Growth Supplement-rat, DMEM medium (Gibco, NY, USA) supplemented with 20% fetal bovine serum (FBS, Gibco, NY, USA), 1% endothelial cell growth supplement-Rat, DMEM supplemented with 20% fetal bovine serum (FBS, Gibco, NY, USA) Cat#1062, Sciencell, USA) and 1% penicillin/streptomycin in an incubator at 5%CO<sub>2</sub>, 37°C.

R-pmvecs were randomly divided into the following five groups: normal control group (CON), in which the cells were cultured in complete medium containing 20% FBS; Lipopolysaccharide (LPS) group, in which cells were exposed to 100 ng/mL LPS for 24 h; LPS+sh-CDK5 knockdown group, in which cells were transfected with plasmids for 48 h and then treated with 100ng/mL LPS for 24 h, and LPS+ QYD group, in which cells were treated with 100ng/mL LPS for 24 h and then treated with QYD for 24 h.

## Transfection

Four sh-RNA sequences targeting the rat CDK5 gene and one negative control interfering sequence that did not match any of the known genes were designed (Suzhou Gemma Genetics Co., Ltd., Suzhou, China), and their corresponding short hairpin structural sequences (sh-CDK5 and sh-NC) were synthesized. The sequences of related gene knockdown are shown in [Supplementary File S2](#). Transfection was performed using a lipid amine TM 2000 transfection reagent (Invitrogen, Carlsbad, California, USA) according to the manufacturer's instructions.

## CCK-8 Assay

CCK-8 kit (Yisheng Biotech Shanghai Co., LTD., Shanghai, China) was used to measure the effect of different QYD concentrations on R-PMVECs viability. The cell suspension was seeded in a 96-well plate and cultured in an incubator for 24 h. The cells were stimulated with different QYD concentrations of 30 ug/mL, 60 ug/mL, 120 ug/mL, 180 ug/mL, and 300 ug/mL, respectively. The medium of each well was removed, the medium containing CCK-8 was added into the incubator for 1.5 h, and a microplate reader measured the absorbance of OD450.

## Immunofluorescence Analysis

Tissue immunofluorescence analysis: 5 µm paraffin sections are dewaxed to water, and serum blockade is performed after antigen retrieval. The primary antibodies against CDK5 and NFAT5 were dropped onto the sections, and the two primary antibodies were mixed and added to the tissues at a certain dilution ratio. The sections were incubated in a wet box overnight at 4°C, and the secondary antibodies were incubated at 37°C for 1 h. The nuclei were then observed using fluorescence microscopy after staining with DAPI (Sigma-Aldrich, St. Louis, Missouri), washed thrice with PBS, and added fluorescent anti-quenching agents.

For immunofluorescence analysis, r-pmvecs were seeded on confocal plates and fixed with 4% paraformaldehyde for 30 minutes, permeabilized with 0.1%Triton X-100 for 5 min, washed with PBS, and blocked with 5% bovine serum albumin (BSA) for 1 h. Cells were incubated with primary antibody Acetyl- $\alpha$ -Tubulin, rhodamine-labeled Phalloidin and incubated overnight at 4°C, washed with PBS, and incubated with secondary antibody for 1 h at 37°C. Nuclei of R-PMVEC were counterstained with DAPI. Imaging was performed by laser confocal microscopy. Images were processed using Image J software to outline cell boundaries and calculate unoccupied areas.

## Statistical Analyses

Experimental data consisted of at least three independent replications and were expressed as standard deviation (SD)  $\pm$  mean. One-way analysis of variance (ANOVA) was used for multiple groups (normally distributed variables). In addition, statistical analyses and visualizations were performed using GraphPad Prism 8.2 and SPSS 24.0. P-values of  $<0.05$  were considered statistically significant (\*P < 0.05, \*\*P < 0.01, \*\*\*P < 0.001).

## Results

### Identification of Prototype Components of QYD in Blood and Critical Targets for SAP Therapy

The chemical components and constituents absorbed into the blood of QYD were obtained from TCMSP and DCABM-TCM databases, respectively. Eighteen compounds were identified as prototype components of QYD that were absorbed into the blood (Figure 1A). A total of 764 targets for 18 prototype components were acquired from the TCMSP, DrugBank, SwissTargetPrediction, and SuperPred databases (Figure 1B) (Supplementary File S3). The GO enrichment analysis revealed that the biological processes influenced by the prototype components mainly included protein phosphorylation, protein autophosphorylation, reaction to external stimuli, and peptide serine phosphorylation (Figure 1C). The KEGG enrichment analysis revealed that the prototype components had a considerable enrichment in signaling pathways related to malignancy, neuroactive ligand-receptor interactions, and resistance to EGFR tyrosine kinase inhibitors (Figure 1D). Using the data provided above, we conducted an intersection analysis of the genes connected to the biological processes of QYD and SAP. Twenty-five genes were shown to be significant candidates for QYD intervention in SAP, as shown in Figure 1E (Supplementary File S4).

### Molecular Docking

The top four docking scores for all interactions between constituents and proteins during the molecular docking process are listed in Figure 2A. The results of the docking of the eighteen components of QYD, the two CDK5 inhibitors, and the

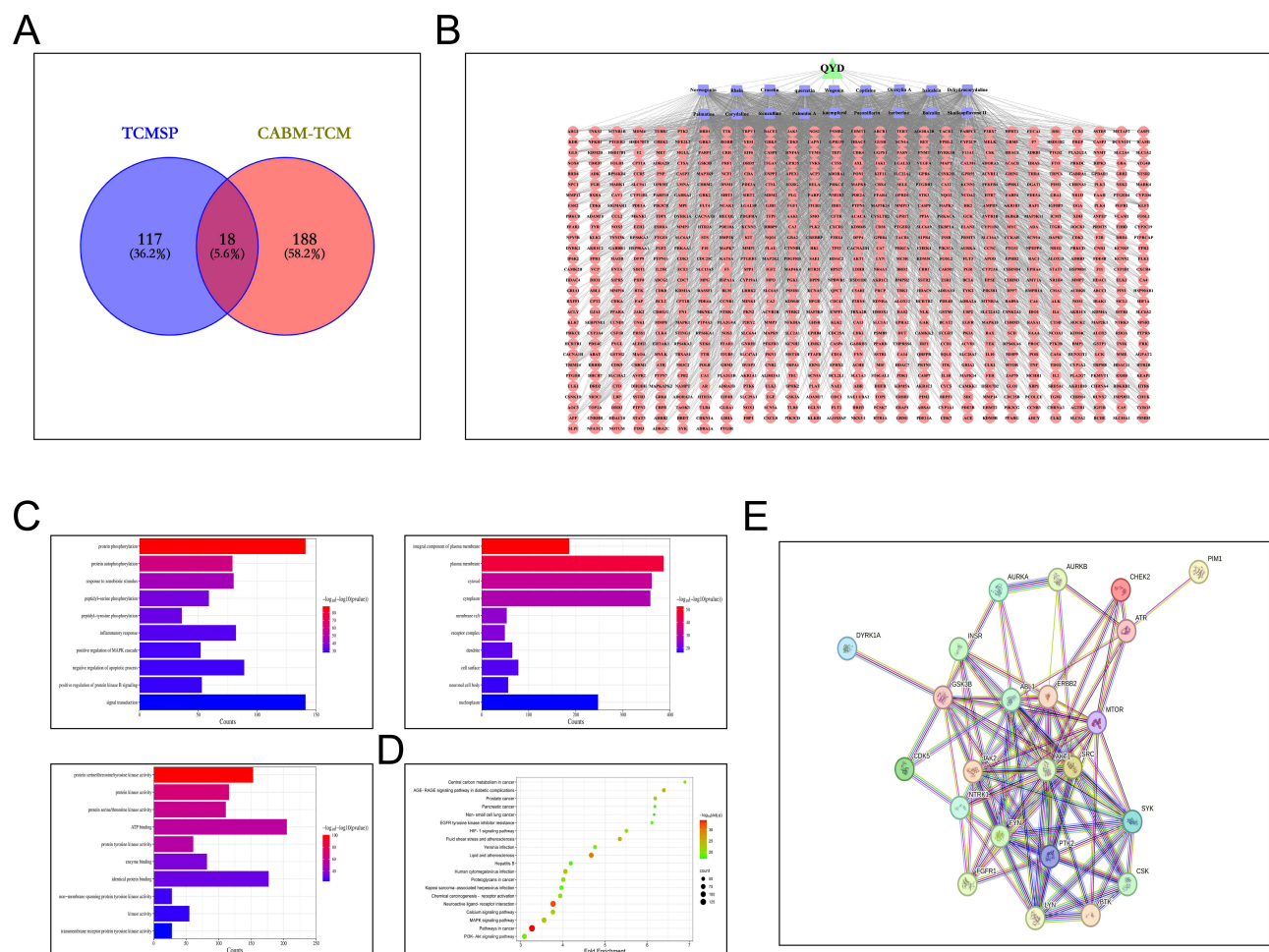


**Figure 1** Identifying prototype components of QYD in blood and critical targets for SAP therapy. (A) Venn diagram illustrating the intersection between QYD chemical components and prototype components. (B) A PPI network of QYD's "component-target". (C) GO enrichment analysis. (D) KEGG enrichment analysis. (E) PPI networks for the key targets.

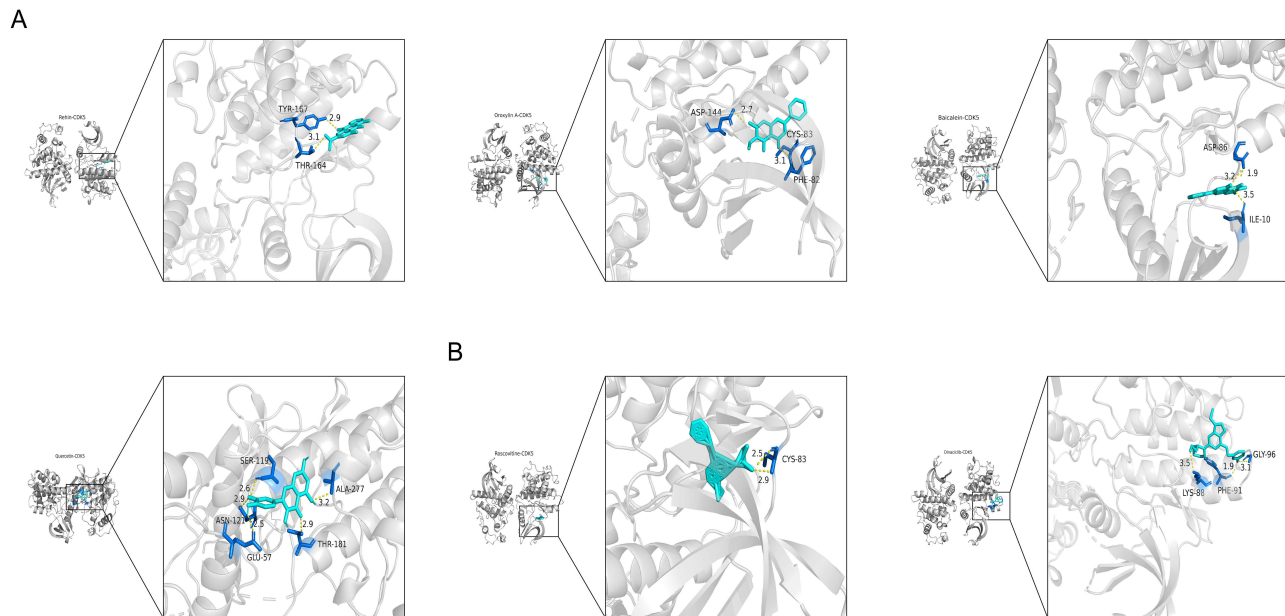


**Figure 2** Molecular docking. **(A)** Molecular docking for Rehin, Oroxlylin A, Baicalein, Quercetin, and CDK5. **(B)** Molecular docking for Roscovitine, Dinaciclib, and CDK5.

CDK5 protein are shown in [Figure 2B](#). According to the research results, each active constituent forms strong hydrogen bonds with its core target and exhibits low binding energy. In conclusion, the prototype constituents of QYD can target CDK5 and influence its activity directly. ([Supplementary File S5](#)).

## CDK5 Expression in the Blood of Individuals with SAP

To investigate the CDK5 gene table differences in SAP patients and corresponding controls, we first downloaded the GSE194331 dataset from the GEO database. The uniform manifold approximation and projection (UMAP) algorithm showed that this data could distinguish between SAP patients and healthy populations ([Figure 3A](#)). A volcano plot, followed by a CDK5 boxplot (Boxplot), demonstrated that CDK5 gene expression was statistically significant in SAP patients and healthy populations ([Figure 3B and C](#)).

## QYD or CDK5 Inhibitors Ameliorated Inflammation and Pancreatic Injury in SAP Rats

When rats were injected with STC into the biliopancreatic duct, the histopathological features of the pancreas in the SAP group showed edema, hemorrhage, inflammatory infiltrates, and alveolar necrosis. After the Roscovitine or QYD

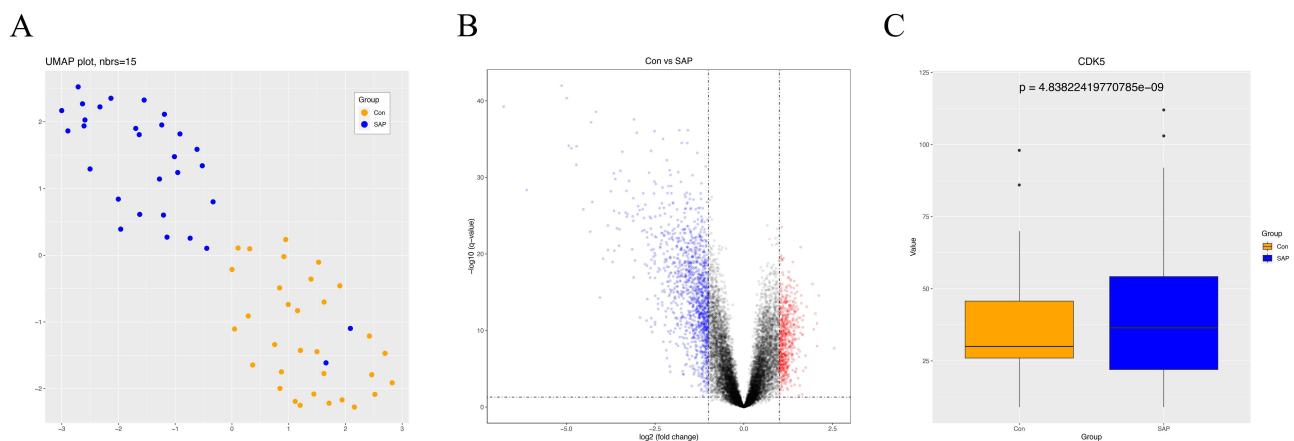


**Figure 3** CDK5 expression in the blood of individuals with SAP. **(A)** Principal component analysis of SAP patient and healthy population data. **(B)** Volcano plot of differentially expressed genes in the GEO dataset. **(C)** Box line plot of CDK5 gene in SAP patients and healthy population.



treatment, the histopathological damage of the pancreas was significantly improved, and the pathological score was lower than that of the SAP group (Figure 4A and B). Serum amylase is a very familiar diagnostic marker for pancreatitis with very high sensitivity and specificity in the early stages of SAP, and the gradual accumulation of inflammatory mediators in the circulation is a crucial step in the progression of the pancreas from localized inflammation to SIRS and MODS. As shown in the result, serum levels of amylase, TNF- $\alpha$ , and IL-6 were higher in the SAP group than in the SO group. In contrast, applying Roscovitine or QYD reduced amylase levels and inflammatory factors (Figure 4C–E).

## QYD or CDK5 Inhibitors Substantially Ameliorated ALI Induced by SAP

We detected secondary ALI in rats induced with SAP. The lungs of the SAP group showed edema, leukocyte infiltrates, hemorrhage, and alveolar septal thickening. In contrast, lung injuries were improved after the Roscovitine or QYD treatment. At the same time, the pathological scores of the lungs in groups Roscovitine or QYD were lower than those in the SAP group (Figure 5A and B). Lung wet/dry weight ratio, bronchoalveolar lavage fluid, and Evans blue dye assay were used to assess pulmonary vascular permeability (Figure 5C–E); these methods showed that pulmonary congestion and edema caused permeability changes in the SAP group, which were alleviated after Roscovitine or QYD treatment.

## Regulatory Effects of QYD or CDK5 Inhibitors on the NFAT5-GEF-H1 Signaling Pathway

Previous experiments have confirmed that CDK5 is an upstream activator of the transcription factor NFAT5, and the upstream-downstream relationship has been validated.<sup>26,27</sup> The result of differential expression analysis performed a correlation between CDK5 and NFAT5 in the gene set of SAP patients, which showed a significant positive correlation (Figure 6A). Based on the PCR and Western Blot results, there was a substantial increase in the mRNA and protein expression of the CDK5 in the lung tissue of SAP rats. The administration of roscovitine or QYD drastically reduced CDK5 expression. To further validate whether ALI is caused by activated CDK5 acting NFAT5 at the onset of SAP, we verified the expression of NFAT5 in different groups. The mRNA and protein expression of NFAT5 in the SAP group were significantly higher than in the SO group, and the results were relieved after treatment with Roscovitine or the

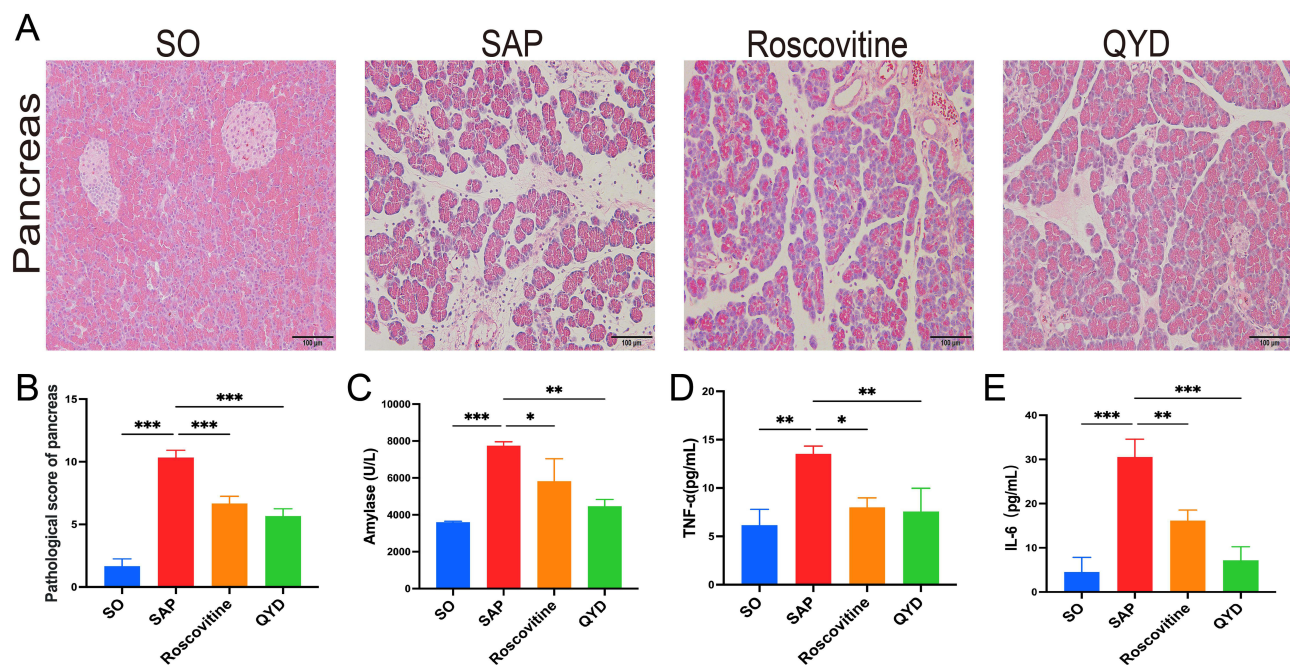


**Figure 4** QYD or CDK5 inhibitors ameliorated inflammation and pancreatic injury in SAP rats. (A) Hematoxylin and eosin (HE) staining was analyzed for pathological changes in pancreatic tissues (scale bar, 100  $\mu$ m). (B) Histopathological scores of pancreatic tissues in each group. (C) Analysis of serum amylase levels. (D and E) Analysis of serum levels of inflammatory factors TNF- $\alpha$  and IL-6 in each group of rats. Data are representative images or expressed as mean  $\pm$  SD from at least three independent experiments in each group of rats; \*P < 0.05, \*\*P < 0.01, \*\*\*P < 0.001.

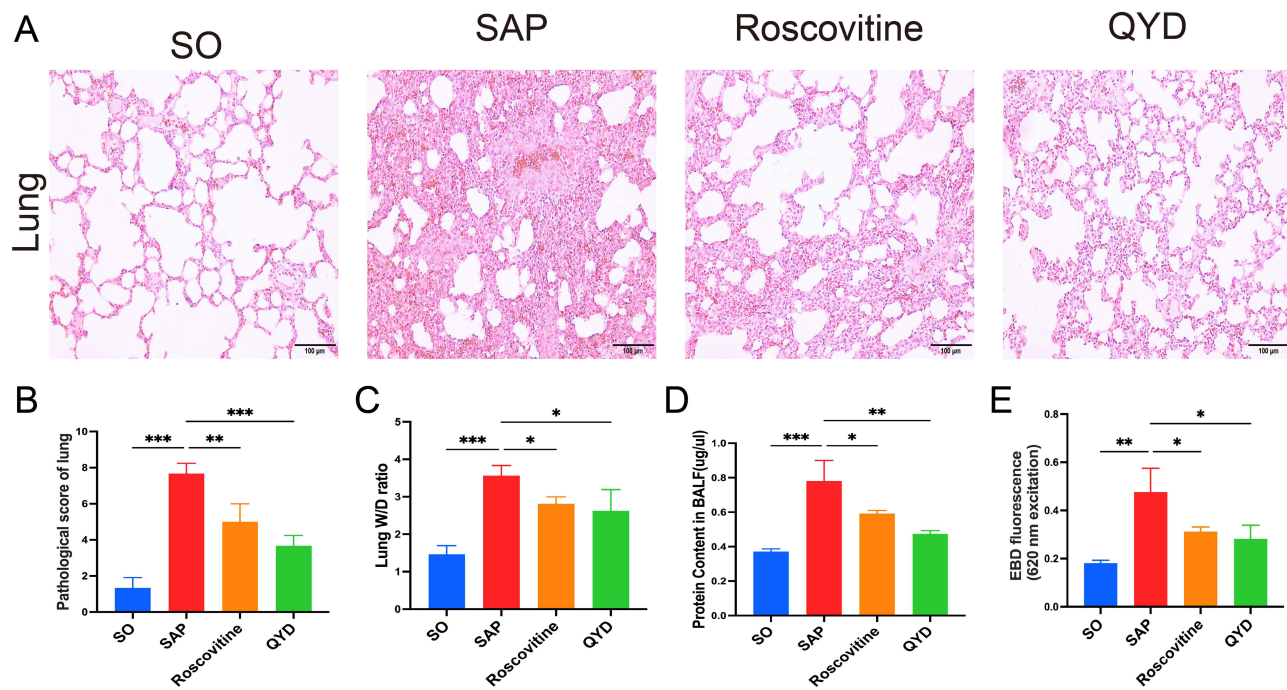


**Figure 5** QYD or CDK5 inhibitors substantially ameliorated ALI induced by SAP. **(A)** Hematoxylin and eosin (HE) staining was analyzed for pathological changes in lung tissues (scale bar, 100  $\mu$ m). **(B)** Histopathological scores of lung tissues in each group. **(C–E)** Representative results of lung wet/dry weight ratios, bronchoalveolar lavage fluid, and Evans blue dye assay in each group. Data are representative images or expressed as mean  $\pm$  SD from at least three independent experiments in each group of rats; \* $P$  < 0.05, \*\* $P$  < 0.01, \*\*\* $P$  < 0.001.

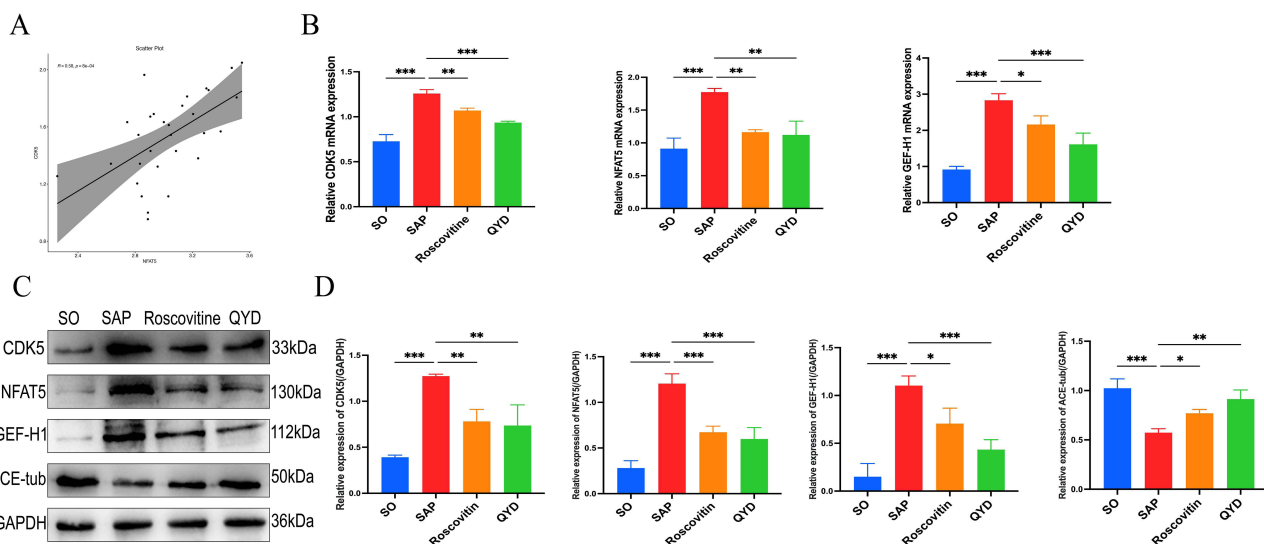


**Figure 6** Regulatory effects of QYD or CDK5 inhibitors on the NFAT5-GEF-H1 signaling pathway. **(A)** Scatter plot of CDK5 and NFAT5 genes in SAP patients. Quantitative RT-PCR analysis of the relative levels of CDK5, NFAT5 and GEF-H1 **(B)** mRNA in rat lung tissues. **(C and D)** Western blot was performed to assess the protein expression levels of CDK5, NFAT5, GEF-H1, and Acetyl-alpha Tubulin in rat lung tissues. GAPDH was used as a loading control. Semi-quantification of protein expression of CDK5, NFAT5, GEF-H1 and Acetyl-alpha Tubulin using histograms. Data are representative images or expressed as mean  $\pm$  SD of each group of rats from at least three independent experiments; \* $P$  < 0.05, \*\* $P$  < 0.01, \*\*\* $P$  < 0.001.

QYD. NFAT5, functioning as a transcription factor, controls cellular homeostasis in reaction to external stressors, namely the production of cytoskeletal proteins.<sup>28,29</sup> Acetyl-alpha Tubulin and guanine nucleotide exchange factor (GEF-H1) are crucial in maintaining microtubule integrity within the cytoskeleton. ALI is a consequence of the expression of microtubule-associated proteins when there is a disruption to microtubule integrity.<sup>30</sup> The mRNA and protein levels of

GEF-H1 in lung tissues across all groups exhibited a pattern comparable to the expression trend of NFAT5. The expression of Acetyl-alpha Tubulin decreased in SAP. However, the expression increased after retreatment with Roscovitine or QYD treatment (Figure 6B–D).

## Lung Tissue Immunofluorescence in Rats

The double immunofluorescence labeling method showed lower expression of CDK5 and NFAT5 in rat lung tissues relative to the SO group. Still, the level of co-localized fluorescence effect was significantly higher in SAP. In contrast, the expression of CDK5 and NFAT5 was reduced after Roscovitine or QYD treatment (Figure 7A–C).

## Protective Effect of QYD or CDK5 Knockdown on Pulmonary Microvascular Endothelial Cell Injury

We used four sh-RNA sequences to achieve CDK5 knockdown. It was found that the mRNA level of CDK5 was significantly reduced in cells transfected with sh-RNAs (sh-CDK5-1, sh-CDK5-2, sh-CDK5-3, and sh-CDK5-4) compared to cells transfected with sh-NC, and sh-CDK5-3 had the best knockdown effect and was continued to be used for subsequent experiments (Supplementary File S2). Afterward, we verified the optimal QYD concentration of R-PMVECs by CCK8 experiments (Figure 8A). 60ug/mL is considered the optimal intervention concentration for QYD. After treatment of R-PMVECs with LPS, we found that the mRNA levels of inflammatory cytokines (TNF- $\alpha$  and IL-6) were significantly reduced after CDK5 knockdown or QYD treatment compared to the LPS+sh-NC group or the LPS group (Figure 8B and C). Since fibronectin (F-actin) and microtubules in the cytoskeleton play a crucial role in regulating the endothelial barrier function, we performed immunofluorescence assays on them, and LPS-induced changes in the structure of F-actin and Acetyl-alpha Tubulin and attenuation of fluorescence intensity. Acetyl-alpha tubulin and F-actin were relieved when CDK5 was knocked down, or QYD treatment was given (Figure 8D–F).

## The Regulatory Effect of QYD or CDK5 Knockdown on NFAT5-GEF-H1 Signaling Pathway

In addition, we also found that CDK5, NFAT5, and GEF-H1 were consistently elevated in mRNA expression compared to the CON group and decreased compared to the LPS+sh-NC group or the LPS group after CDK5 knockdown or QYD treatment (Figure 9A). Similarly, Western blot results showed that when CDK5 was depleted, or after QYD treatment, the expression of CDK5, NFAT5, and GEF-H1 was decreased compared to the LPS+sh-NC group or the LPS group, and the expression of Acetyl-alpha Tubulin protein showed an opposite trend (Figure 9B and C). The above findings suggest that CDK5 is involved in the LPS-stimulated inflammatory response and that CDK5 downregulation alleviates the progression of the inflammatory response. In addition, QYD attenuated the damage induced by LPS activation of CDK5/NFAT5/GEF-H1 signaling in R-PMVECs by regulating the cytoskeleton.

## Discussion

SAP is an inflammatory disease caused by multiple factors. Over time, if not treated promptly, the inflammatory response usually accumulates throughout the body, leading to multi-organ failure or causing infectious necrosis of the pancreas, which in turn induces more severe complications such as acute respiratory distress syndrome, gastrointestinal bleeding, and shock.<sup>31,32</sup> The clinical management of SAP has been a significant challenge in the past few years. Although the treatment of SAP in the clinic has gained strong support in recent years, clarifying the exact pathogenesis of the disease remains a pressing issue. QYD has been validated in treating SAP-associated intestinal barrier and myocardial injury.<sup>18,33</sup> However, treatment in the direction of SAP-ALI, which is responsible for 60–70% of SAP-related deaths, still requires in-depth study.<sup>8</sup> The pathogenesis of ALI secondary to SAP, which is a form of secondary lung injury, remains to be further investigated. Currently, the prevailing mechanism is that pancreatitis-associated inflammatory factors enter the bloodstream and pass through the pulmonary circulation to disrupt the air-blood barrier of the lungs, generating many injury-associated molecular patterns leading to lung parenchymal cell injury. In addition, researchers have identified extracellular vesicle ITGAM and ITGB2 as being important in the pathogenesis of lung injury secondary to SAP.<sup>34</sup> In

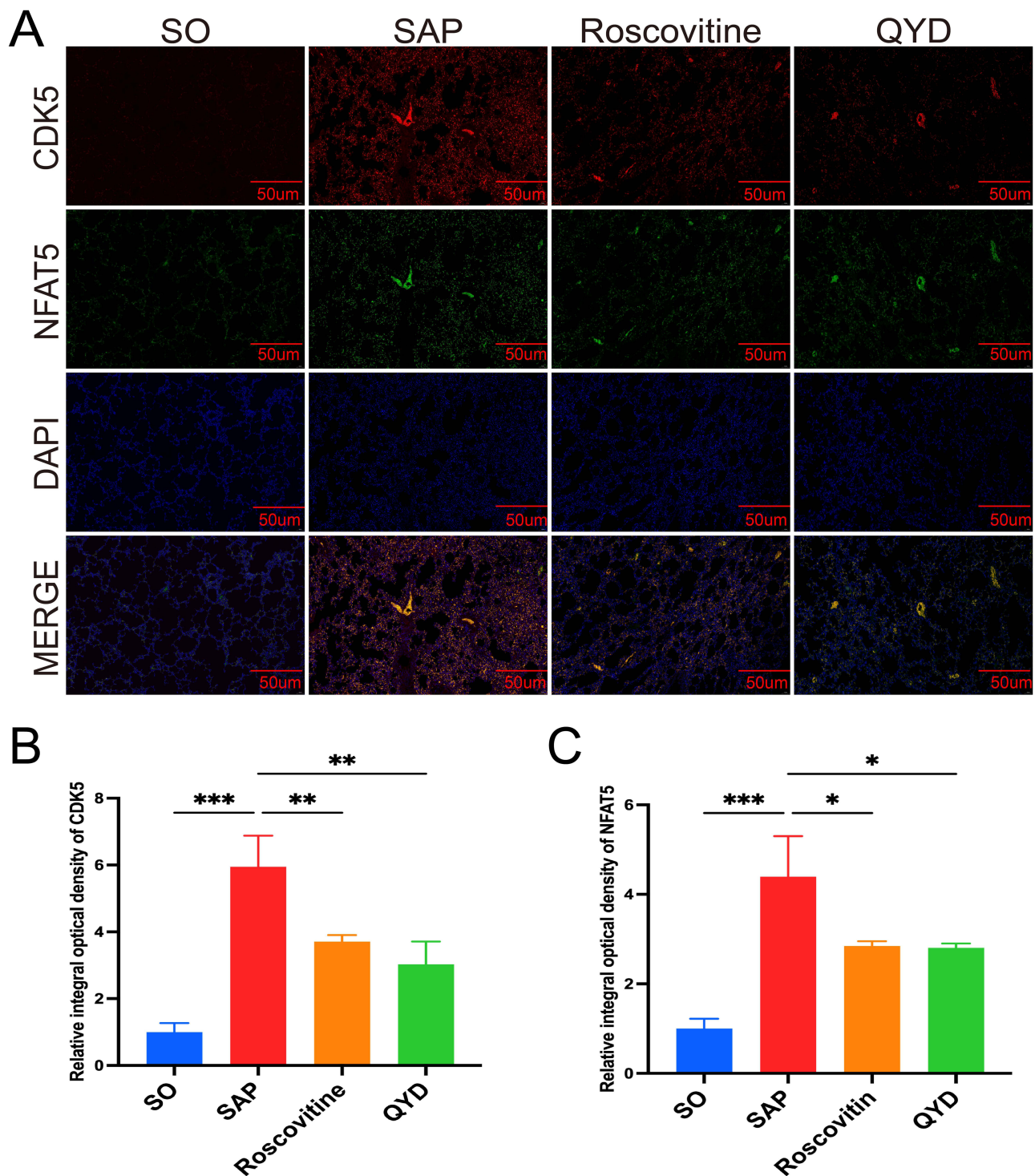


**Figure 7** Lung tissue immunofluorescence in rats. (A) Immunofluorescence analysis of CDK5 (red), NFAT5 (green), and nucleus (blue) expression in lung tissue (scale bar=50µm). (B and C) Semi-quantitative analysis of CDK5 and NFAT5 expression; \* $P < 0.05$ , \*\* $P < 0.01$ , \*\*\* $P < 0.001$ .

this study, STC retrograde biliopancreatic duct injection induced a stable and reliable model of pancreatic and lung injury in rats. QYD effectively alleviated SAP and SAP-related acute lung injuries, reduced inflammation and pulmonary edema, and restored their ventilatory function.

ALI is characterized by rupture of the alveolar-capillary barrier, increased permeability of endothelial and epithelial cells, reduced lung compliance, and impaired gas exchange, resulting in diffuse interstitial and alveolar edema.<sup>35</sup>

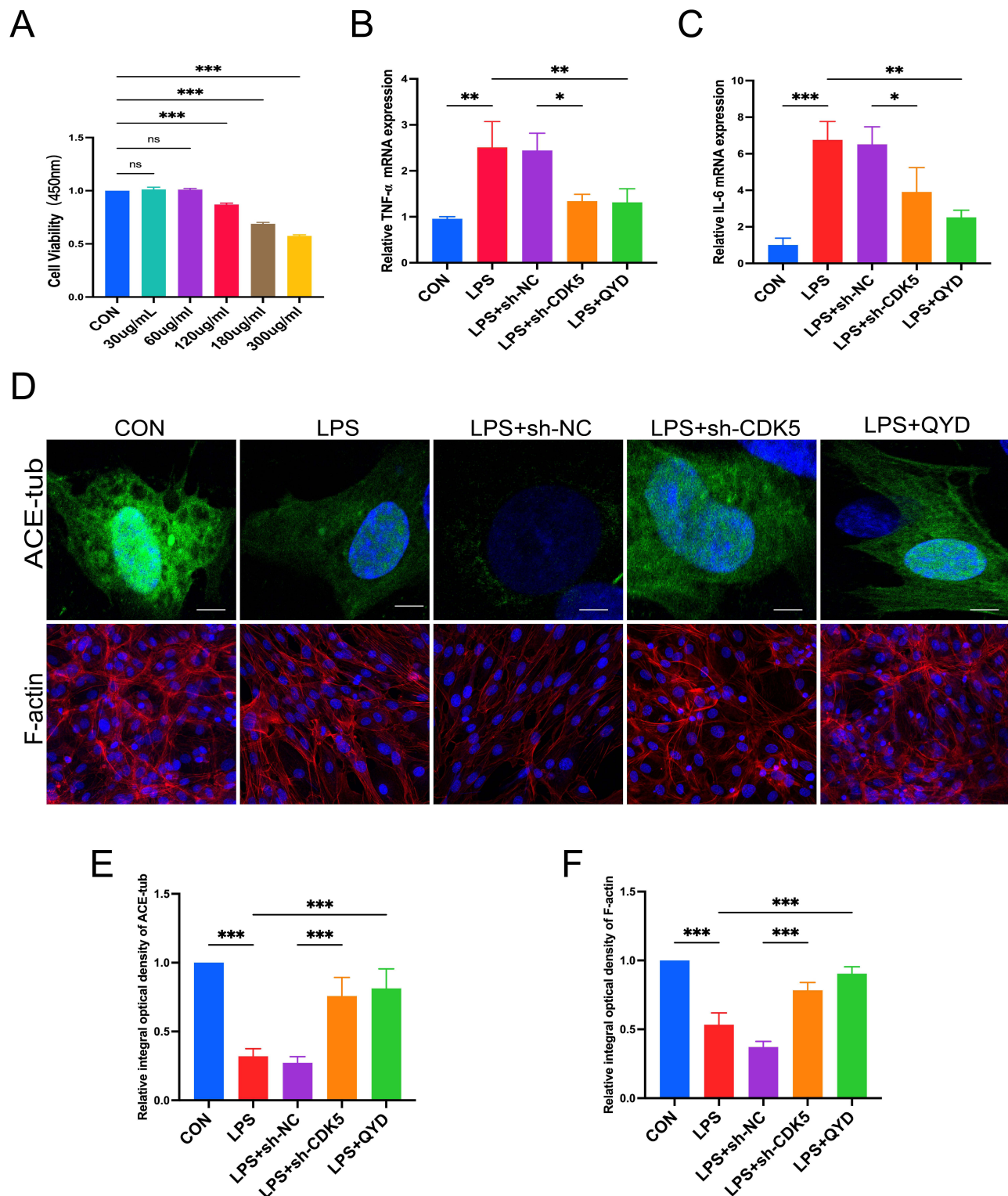


**Figure 8** Protective effect of QYD or CDK5 knockdown on pulmonary microvascular endothelial cell injury. (A) Detection of r-PMVEC optimal QYD concentration by CCK8. (B and C) Inflammatory cytokine TNF- $\alpha$  and IL-6 mRNA levels were assessed by RT-qPCR of their histograms in response to LPS-induced treatment with sh-CDK5 or QYD in r-PMVEC. (D–F) Immunofluorescence staining and semi-quantitative analysis of different groups of R-PMVEC cytoskeleton F-actin and Acetyl-alpha Tubulin (scale bar = 20 $\mu$ m; scale bar = 10 $\mu$ m). Data are representative images or expressed as from at least three independent experiments; \*P < 0.05, \*\*P < 0.01, \*\*\*P < 0.001.

Pulmonary microvascular endothelial cells are the main target of humoral and cellular mediators during injury.<sup>17,30,36</sup> Existing studies have indicated that SNHG3 can regulate the barrier permeability of the pulmonary microvascular endothelial barrier in ALI, and downregulation of SNHG3 may play a role in repairing the endothelial barrier.<sup>37</sup>

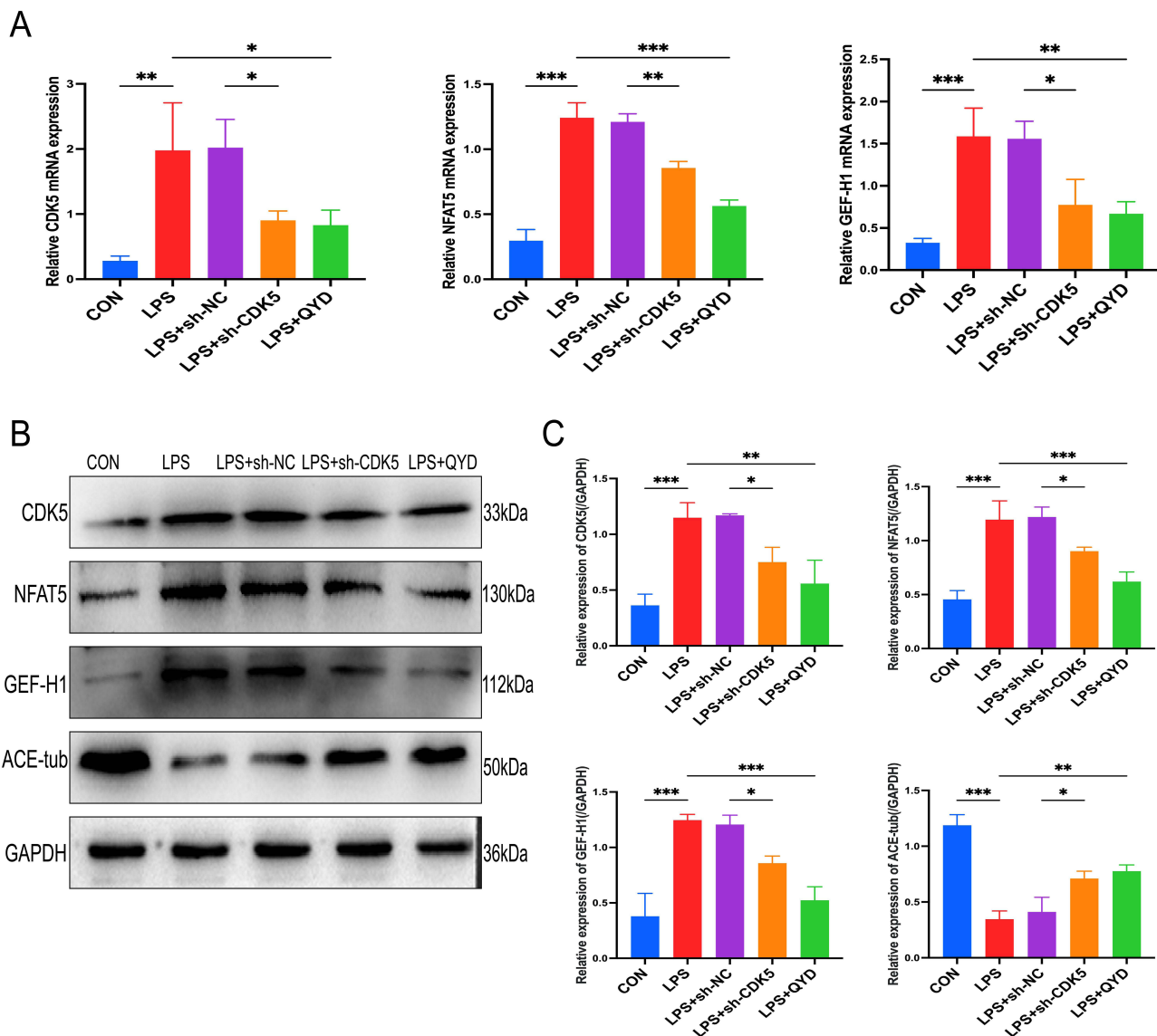


**Figure 9** The regulatory effect of QYD or CDK5 knockdown on NFAT5-GEF-H1 signaling pathway. **(A)** Quantitative RT-PCR was performed to analyze the relative levels of CDK5, NFAT5, and GEF-H1 in r-PMVEC. **(B and C)** Western blot and histograms were performed to assess the protein expression levels of CDK5, NFAT5, GEF-H1, and Acetyl-alpha Tubulin, and GAPDH was used as a loading control. Data are representative images or expressed as from at least three independent experiments; \* $P < 0.05$ , \*\* $P < 0.01$ , \*\*\* $P < 0.001$ .

Downregulation of RIP140 could alleviate LPS-induced Human Pulmonary microvascular endothelial cells (h-PMVECs) inflammation, apoptosis, and permeability by regulating CTBP2.<sup>38</sup> The ROCK inhibitor fasudil reduces the expression of inflammatory factors in LPS-induced rat lung microvascular endothelial cells via the ROS/NF- $\kappa$ B pathway.<sup>39</sup> Therefore, PMVECs are essential to preventing the development of SAP-associated ALI.

CDK5 is a specific member of the cell cycle protein kinase family, which was initially found to have a particular activity in the nervous system and has been closely associated with neurodevelopment and the development of various brain diseases.<sup>40</sup> In addition, it plays an essential regulatory role in cytoskeletal actin dynamics and microtubule stability.<sup>41–43</sup> With increasing research, relevant studies have revealed the involvement of CDK5 in the immune-inflammatory response. In toll-like receptor-stimulated primary macrophages, both CDK5 knockdown or knockout of its activator p35 lead to increased macrophage interleukin-10 production and lead to immunosuppression.<sup>44</sup> CDK5 deficiency enhances the anti-inflammatory potential of glucocorticoid-mediated glucocorticoid receptor activation during inflammation.<sup>45</sup> NFAT5 is a member of the nuclear factor transcription factor family of activated T cells and regulates

osmotic stress-induced gene expression in mammalian cells.<sup>46</sup> Researchers have demonstrated that NFAT5 can participate in the immune response independently of osmotic stress. The role of NFAT5 as a promoter of pro-inflammatory macrophage function has been shown in mouse models and studies of human rheumatoid arthritis patients.<sup>11,47</sup> In addition, NFAT5 participates in sepsis immunoregulation in the form of complexes.<sup>48</sup>

A cytoskeleton is an intracellular network structure with protein fibers as its main component, mainly composed of three types of protein fibers: microtubules, microfilaments, and intermediate fibers. The essential part of microtubules is microtubulin ( $\alpha$ -microtubulin and  $\beta$ -microtubulin form microtubulin dimers), the integral component of microfilaments is actin, and the essential element of intermediate fibers is relatively more complex, containing a class of fibronectin family. Due to the complex tertiary structure of the cytoskeleton, its form plays an essential regulatory role in the cell, ensuring that the life activities of the organelles are carried out in a normal and orderly manner, providing mechanical support for the intracellular transport of substances and organelles and movement, providing mechanical power for cellular motility, and participating in cell division and secretion, receptor signaling, etc.<sup>49,50</sup> As the research progressed, researchers found that the actin cytoskeleton controls inflammation by regulating the activation of immune cells and the permeability of the epithelial and endothelial barriers.<sup>51</sup> Microtubules regulate pathogen sensing through inflammatory vesicles, assembly of immune synapses, and vascular leakage in inflamed tissues.<sup>52</sup> Acetyl-alpha Tubulin, a modification of microtubules, reflects the degree of microtubule stability.<sup>14,53</sup> Therefore, we investigated the role of QYD in regulating the microtubule structure by immunofluorescence and Western Blot. GEF-H1, as a microtubule-interacting protein, and the stability of microtubules have demonstrated that the exchange activity of GEF-H1 is inhibited in its microtubule homeostatic state. When the outside world stimulates the microtubules, the homeostasis is disrupted, and GEF-H1 is released from the microtubules and stimulates its downstream RhoA-specific GEF activity, thereby causing endothelial barrier function destruction and inflammatory response.<sup>54</sup>

CDK5, an activator of the transcription factor NFAT5, regulates NFAT5 transcription and has been confirmed to be active in osmotic pressure.<sup>26,27,55</sup> Whether CDK5 acts NFAT5 to cause cytoskeleton changes has yet to be verified in the SAP-ALI model. Our study discovered a considerable increase in CDK5 levels in the blood of individuals with SAP. Furthermore, CDK5 showed a strong affinity with 18 prototype components. The techniques of HE staining, qPCR, Western blot, and immunofluorescence were used to ascertain the pivotal function of CDK5 in the degradation of the microtubule in rat pulmonary microvascular endothelial cells produced by SAP. In addition, QYD may alleviate SAP-ALI by adjusting microtubule stability in the CDK5/NFAT5/GEF-H1 signaling pathway. However, there are still some shortcomings in our study, and this study was limited to rats for in vitro and in vivo experiments. Still, it is not clear whether the results can be validated in SAP-ALI patients. Therefore, our follow-up needs to focus on addressing these shortcomings.

## Conclusion

To summarize, we have found 18 constituents of QYD absorbed into the blood that exhibit pharmacological actions related to anti-inflammatory and immunological modulation. CDK5 was recognized as a pivotal protein in the QYD therapy of SAP-induced pulmonary microvascular endothelial cell damage. CDK5 may enhance the microtubule disassembly mediated by GEF-H1 and increase the permeability of lung endothelial cells by activating NFAT5 during SAP. The potential of QYD as a CDK5 inhibitor has been established, and it may reduce SAP-associated ALI by acting in the NFAT5-GEF-H1 signaling pathway. Ultimately, there remain certain limitations in our research, as we have only conducted a preliminary exploration of the QYD's effects on the CDK5/NFAT5/GEF-H1 signaling pathway. In subsequent studies, we will further investigate the effects of the effective monomeric components of QYD on this pathway in depth, and conduct positive and negative validation through follow-up rescue experiments.

## Data Sharing Statement

The original data for this study can be obtained from the GEO public database (<https://www.ncbi.nlm.nih.gov/geo/>).

## Acknowledgments

The author would like to thank Dr. Anliang Huang for his bioinformatics data analysis of the article, as well as Figdraw for abstract graph support.

## Funding

This study was supported by the National Natural Science Foundation of China (No. 82274311 and No.82074158), and the National Key R&D Program of China (No. 2019YFE0119300).

## Disclosure

The authors report no conflicts of interest in this work.

## References

1. Garg PK, Singh VP. Organ failure due to systemic injury in acute pancreatitis. *Gastroenterology*. 2019;156(7):2008–2023. doi:10.1053/j.gastro.2018.12.041
2. Lee PJ, Papachristou GI. New insights into acute pancreatitis. *Nat Rev Gastroenterol Hepatol*. 2019;16(8):479–496. doi:10.1038/s41575-019-0158-2
3. Barreto SG, Habtezion A, Gukovskaya A, et al. Critical thresholds: key to unlocking the door to the prevention and specific treatments for acute pancreatitis. *Gut*. 2021;70(1):194–203. doi:10.1136/gutjnl-2020-322163
4. van Santvoort HC, Bakker OJ, Bollen TL, et al. A conservative and minimally invasive approach to necrotizing pancreatitis improves outcome. *Gastroenterology*. 2011;141(4):1254–1263. doi:10.1053/j.gastro.2011.06.073
5. Wu J, Zhang J, Zhao J, Chen S, Zhou T, Xu J. Treatment of severe acute pancreatitis and related lung injury by targeting gasdermin D-mediated pyroptosis. *Front Cell Dev Biol*. 2021;9:780142. doi:10.3389/fcell.2021.780142
6. Baron TH, DiMaio CJ, Wang AY, Morgan KA. American gastroenterological association clinical practice update: management of pancreatic necrosis. *Gastroenterology*. 2020;158(1):67–75.e1. doi:10.1053/j.gastro.2019.07.064
7. Dhariwala FA, Rajadhyaksha MS. An unusual member of the Cdk family: cdk5. *Cell Mol Neurobiol*. 2008;28(3):351–369. doi:10.1007/s10571-007-9242-1
8. Xu J, Tsutsumi K, Tokuraku K, Estes KA, Hisanaga S, Ikezu T. Actin interaction and regulation of cyclin-dependent kinase 5/p35 complex activity. *J Neurochem*. 2011;116(2):192–204. doi:10.1111/j.1471-4159.2010.06824.x
9. Xie Z, Samuels BA, Tsai LH. Cyclin-dependent kinase 5 permits efficient cytoskeletal remodeling—a hypothesis on neuronal migration. *Cereb Cortex*. 2006;16 Suppl 1:i64–i68. doi:10.1093/cercor/bhj170
10. Pfänder P, Eiers AK, Burret U, Vettorazzi S. Deletion of Cdk5 in macrophages ameliorates anti-inflammatory response during endotoxemia through induction of C-Maf and Il-10. *Int J Mol Sci*. 2021;22(17). doi:10.3390/ijms22179648
11. Choi S, You S, Kim D, et al. Transcription factor NFAT5 promotes macrophage survival in rheumatoid arthritis. *J Clin Invest*. 2017;127(3):954–969. doi:10.1172/jci87880
12. Gwon DH, Kim SI, Lee SH, et al. NFAT5 deficiency alleviates formalin-induced inflammatory pain through mTOR. *Int J Mol Sci*. 2021;22(5). doi:10.3390/ijms22052587
13. Mottahedin A, Joakim Ek C, Truvé K, Hagberg H, Mallard C. Choroid plexus transcriptome and ultrastructure analysis reveals a TLR2-specific chemotaxis signature and cytoskeleton remodeling in leukocyte trafficking. *Brain Behav Immun*. 2019;79:216–227. doi:10.1016/j.bbi.2019.02.004
14. Kratzer E, Tian Y, Sarich N, et al. Oxidative stress contributes to lung injury and barrier dysfunction via microtubule destabilization. *Am J Respir Cell Mol Biol*. 2012;47(5):688–697. doi:10.1165/rcmb.2012-0161OC
15. Azoitei ML, Noh J, Marston DJ, et al. Spatiotemporal dynamics of GEF-H1 activation controlled by microtubule- and Src-mediated pathways. *J Cell Biol*. 2019;218(9):3077–3097. doi:10.1083/jcb.201812073
16. Wei TF, Zhao L, Huang P, et al. Qing-Yi decoction in the treatment of acute pancreatitis: an integrated approach based on chemical profile, network pharmacology, molecular docking and experimental evaluation. *Front Pharmacol*. 2021;12:590994. doi:10.3389/fphar.2021.590994
17. Yang YS, Chen K, Xie WR, Wang H. 清胰颗粒对重症急性胰腺炎大鼠肝、肾组织HMGB1表达的影响 [Effect of Qingyi Granule on HMGB1 expression in liver and renal tissues of severe acute pancreatitis rats]. *Zhongguo Zhong Xi Yi Jie He Za Zhi*. 2015;35(11):1367–1372. Chinese.
18. Zhang JW, Zhang GX, Chen HL, et al. Therapeutic effect of Qingyi decoction in severe acute pancreatitis-induced intestinal barrier injury. *World J Gastroenterol*. 2015;21(12):3537–3546. doi:10.3748/wjg.v21.i12.3537
19. Su S, Liang T, Zhou X, He K, Li B, Xia X. Qingyi decoction attenuates severe acute pancreatitis in rats via inhibition of inflammation and protection of the intestinal barrier. *J Int Med Res*. 2019;47(5):2215–2227. doi:10.1177/0300060518809289
20. Sherman BT, Hao M, Qiu J, et al. DAVID: a web server for functional enrichment analysis and functional annotation of gene lists (2021 update). *Nucleic Acids Res*. 2022;50(W1):W216–W221. doi:10.1093/nar/gkac194
21. Sato S, Nakamura F, Hiroshima Y, et al. Caerulein-induced pancreatitis augments the expression and phosphorylation of collapsin response mediator protein 4. *J Hepatobiliary Pancreat Sci*. 2016;23(7):422–431. doi:10.1002/jhbp.361
22. Trott O, Olson AJ. AutoDock Vina: improving the speed and accuracy of docking with a new scoring function, efficient optimization, and multithreading. *J Comput Chem*. 2010;31(2):455–461. doi:10.1002/jcc.21334
23. Rongione AJ, Kusske AM, Kwan K, Ashley SW, Reber HA, McFadden DW. Interleukin 10 reduces the severity of acute pancreatitis in rats. *Gastroenterology*. 1997;112(3):960–967. doi:10.1053/gast.1997.v112.pm9041259
24. Osman MO, Kristensen JU, Jacobsen NO, et al. A monoclonal anti-interleukin 8 antibody (WS-4) inhibits cytokine response and acute lung injury in experimental severe acute necrotizing pancreatitis in rabbits. *Gut*. 1998;43(2):232–239. doi:10.1136/gut.43.2.232
25. Matute-Bello G, Downey G, Moore BB, et al. An official American Thoracic Society workshop report: features and measurements of experimental acute lung injury in animals. *Am J Respir Cell Mol Biol*. 2011;44(5):725–738. doi:10.1165/rcmb.2009-0210ST



26. Gallazzini M, Heussler GE, Kunin M, Izumi Y, Burg MB, Ferraris JD. High NaCl-induced activation of CDK5 increases phosphorylation of the osmoprotective transcription factor TonEBP/OREBP at threonine 135, which contributes to its rapid nuclear localization. *Mol Biol Cell.* 2011;22(5):703–714. doi:10.1091/mbc.E10-08-0681
27. Li J, Wang X, Lan T, et al. CDK5/NFAT5-Regulated Transporters Involved in Osmoregulation in *Fejervarya cancrivora*. *Biology.* 2022;11(6). doi:10.3390/biology11060858
28. Lopez-Rodríguez C, Aramburu J, Rakeman AS, Rao A. NFAT5, a constitutively nuclear NFAT protein that does not cooperate with Fos and Jun. *Proc Natl Acad Sci U S A.* 1999;96(13):7214–7219. doi:10.1073/pnas.96.13.7214
29. Madonna R, Doria V, Görbe A, et al. Co-expression of glycosylated aquaporin-1 and transcription factor NFAT5 contributes to aortic stiffness in diabetic and atherosclerosis-prone mice. *J Cell Mol Med.* 2020;24(5):2857–2865. doi:10.1111/jcmm.14843
30. Mu S, Liu Y, Jiang J, et al. Unfractionated heparin ameliorates pulmonary microvascular endothelial barrier dysfunction via microtubule stabilization in acute lung injury. *Respir Res.* 2018;19(1):220. doi:10.1186/s12931-018-0925-6
31. Ke L, Zhou J, Mao W, et al. Immune enhancement in patients with predicted severe acute necrotising pancreatitis: a multicentre double-blind randomised controlled trial. *Intensive Care Med.* 2022;48(7):899–909. doi:10.1007/s00134-022-06745-7
32. Nesvaderani M, Dhillon BK, Chew T, et al. Gene expression profiling: identification of novel pathways and potential biomarkers in severe acute pancreatitis. *J Am Coll Surg.* 2022;234(5):803–815. doi:10.1097/xcs.000000000000115
33. Li L, Li YQ, Sun ZW, et al. Qingyi decoction protects against myocardial injuries induced by severe acute pancreatitis. *World J Gastroenterol.* 2020;26(12):1317–1328. doi:10.3748/wjg.v26.i12.1317
34. Hu Q, Zhang S, Yang Y, et al. Extracellular vesicle ITGAM and ITGB2 mediate severe acute pancreatitis-related acute lung injury. *ACS Nano.* 2023;17(8):7562–7575. doi:10.1021/acsnano.2c12722
35. Confalonieri M, Salton F, Fabiano F. Acute respiratory distress syndrome. *Eur Respir Rev.* 2017;26(144). doi:10.1183/16000617.0116-2016
36. Rizzo MT, Leaver HA. Brain endothelial cell death: modes, signaling pathways, and relevance to neural development, homeostasis, and disease. *Mol Neurobiol.* 2010;42(1):52–63. doi:10.1007/s12035-010-8132-6
37. Wu Y, Li M, Bai J, Ma X. Silencing long non-coding RNA SNHG3 repairs the dysfunction of pulmonary microvascular endothelial barrier by regulating miR-186-5p/Wnt axis. *Biochem Biophys Res Commun.* 2023;639:36–45. doi:10.1016/j.bbrc.2022.11.067
38. Wang Q, Wu Q. Knockdown of receptor interacting protein 140 (RIP140) alleviated lipopolysaccharide-induced inflammation, apoptosis and permeability in pulmonary microvascular endothelial cells by regulating C-terminal binding protein 2 (CTBP2). *Bioengineered.* 2022;13(2):3981–3992. doi:10.1080/21655979.2022.2031403
39. Liu H, Pan Z, Ma X, et al. ROCK inhibitor fasudil reduces the expression of inflammatory factors in LPS-induced rat pulmonary microvascular endothelial cells via ROS/NF- $\kappa$ B pathway. *BMC Pharmacol Toxicol.* 2022;23(1):24. doi:10.1186/s40360-022-00565-7
40. Ao C, Li C, Chen J, Tan J, Zeng L. The role of Cdk5 in neurological disorders. *Front Cell Neurosci.* 2022;16:951202. doi:10.3389/fncel.2022.951202
41. Humbert S, Dhavan R, Tsai L. p39 activates cdk5 in neurons, and is associated with the actin cytoskeleton. *J Cell Sci.* 2000;113(Pt 6):975–983. doi:10.1242/jcs.113.6.975
42. Wada Y, Ishiguro K, Itoh TJ, et al. Microtubule-stimulated phosphorylation of tau at Ser202 and Thr205 by cdk5 decreases its microtubule nucleation activity. *J Biochem.* 1998;124(4):738–746. doi:10.1093/oxfordjournals.jbchem.a022174
43. Reinhardt L, Kordes S, Reinhardt P, et al. Dual Inhibition of GSK3 $\beta$  and CDK5 protects the cytoskeleton of neurons from neuroinflammatory-mediated degeneration in vitro and in vivo. *Stem Cell Rep.* 2019;12(3):502–517. doi:10.1016/j.stemcr.2019.01.015
44. Na YR, Jung D, Gu GJ, Jang AR, Suh YH, Seok SH. The early synthesis of p35 and activation of CDK5 in LPS-stimulated macrophages suppresses interleukin-10 production. *Sci Signal.* 2015;8(404):ra121. doi:10.1126/scisignal.aab3156
45. Pfänder P, Fidan M, Burret U, Lipinski L, Vettorazzi S. cdk5 deletion enhances the anti-inflammatory potential of GC-mediated GR activation during inflammation. *Front Immunol.* 2019;10:1554. doi:10.3389/fimmu.2019.01554
46. Seeger H, Kitterer D, Latus J, Alscher MD, Braun N, Segerer S. The potential role of NFAT5 and osmolarity in peritoneal injury. *Biomed Res Int.* 2015;2015:578453. doi:10.1155/2015/578453
47. Halterman JA, Kwon HM, Leitinger N, Wamhoff BR. NFAT5 expression in bone marrow-derived cells enhances atherosclerosis and drives macrophage migration. *Front Physiol.* 2012;3:313. doi:10.3389/fphys.2012.00313
48. Xu J, Gao C, He Y, et al. NLRC3 expression in macrophage impairs glycolysis and host immune defense by modulating the NF- $\kappa$ B-NFAT5 complex during septic immunosuppression. *Mol Ther.* 2023;31(1):154–173. doi:10.1016/j.ymthe.2022.08.023
49. Hohmann T, Dehghani F. The Cytoskeleton-A complex interacting meshwork. *Cells.* 2019;8(4):362.
50. Tang DD, Gerlach BD. The roles and regulation of the actin cytoskeleton, intermediate filaments and microtubules in smooth muscle cell migration. *Respir Res.* 2017;18(1):54. doi:10.1186/s12931-017-0544-7
51. Lechuga S, Ivanov AI. Disruption of the epithelial barrier during intestinal inflammation: quest for new molecules and mechanisms. *Biochim Biophys Acta Mol Cell Res.* 2017;1864(7):1183–1194. doi:10.1016/j.bbamcr.2017.03.007
52. Ivanov AI, Le HT, Naydenov NG, Rieder F. Novel functions of the septin cytoskeleton: shaping up tissue inflammation and fibrosis. *Am J Pathol.* 2021;191(1):40–51. doi:10.1016/j.ajpath.2020.09.007
53. Tian X, Tian Y, Moldobaeva N, Sarich N, Birukova AA. Microtubule dynamics control HGF-induced lung endothelial barrier enhancement. *PLoS One.* 2014;9(9):e105912. doi:10.1371/journal.pone.0105912
54. Krendel M, Zenke FT, Bokoch GM. Nucleotide exchange factor GEF-H1 mediates cross-talk between microtubules and the actin cytoskeleton. *Nat Cell Biol.* 2002;4(4):294–301. doi:10.1038/ncb773
55. Jeon US, Kim JA, Sheen MR, Kwon HM. How tonicity regulates genes: story of TonEBP transcriptional activator. *Acta Physiol.* 2006;187(1–2):241–247. doi:10.1111/j.1748-1716.2006.01551.x

Journal of Inflammation Research

Dovepress

## Publish your work in this journal

The Journal of Inflammation Research is an international, peer-reviewed open-access journal that welcomes laboratory and clinical findings on the molecular basis, cell biology and pharmacology of inflammation including original research, reviews, symposium reports, hypothesis formation and commentaries on: acute/chronic inflammation; mediators of inflammation; cellular processes; molecular mechanisms; pharmacology and novel anti-inflammatory drugs; clinical conditions involving inflammation. The manuscript management system is completely online and includes a very quick and fair peer-review system. Visit <http://www.dovepress.com/testimonials.php> to read real quotes from published authors.

Submit your manuscript here: <https://www.dovepress.com/journal-of-inflammation-research-journal>